# Dynamic Estimation of Electrical Demand in Hot Rolling Mills

Gonzalo Alonso Orcajo, Josué Rodríguez D., Pablo Ardura G., José M. Cano, *Member, IEEE*, Joaquín G. Norniella, Rocio Llera T., and Diego Cifrián R.

***Abstract*—This paper proposes a method capable of reproducing the particular operating conditions of a hot strip mill and predicting the evolution of the main electrical variables from both the characteristics of the steel to be milled and the specific features of the rolling mill. The method analyzes the load torque and the motor-speed evolution in the stands of the roughing and finishing mill drives, according to the steel to be milled. In this study, three types of carbon alloy steel are considered, thus involving dissimilar hardness characteristics. The main stands of the mill, the power network, and the filter banks have been modeled. The relationship between the grade of steel and both the electrical demand and various power quality parameters is discussed. The results can be used as a part of an expert system for the automatic estimation of the electrical demand in a hot rolling mill.**

***Index Terms*—Electrical demand, finishing mill, hot rolling mill, power system harmonics, roughing mill, steel.**

## I. Introduction

STEELMAKING is an energy-intensive process. Although the majority of energy is consumed by the upstream processes (e.g., blast furnaces, basic oxygen furnaces, and electrical arc furnaces), the energy consumption in the downstream mills is far from insignificant. Out of the downstream processes, the hot rolling operation is certainly the largest consumer of energy, both in the form of fuel gas and electricity.

The electrical consumption in the hot rolling operation is more than 70 kWh/ton. The main consumers are the rolling stands and the coilers. However, auxiliary equipment cannot be neglected because it represents 25% of the electrical energy [1], [2].

Manuscript received July 22, 2015; revised February 2, 2016; accepted February 3, 2016. Date of publication February 23, 2016; date of current version May 18, 2016. Paper 2015-METC-0373.R1, presented at the 2015 IEEE Industry Applications Society Annual Meeting, Addison, TX, USA, October 18–22, and approved for publication in the IEEE TRANSACTIONS ON INDUSTRY APPLICATIONS by the Metals Industry Committee of the IEEE Industry Applications Society. This work was supported in part by the Research and Development Center of ArcelorMittal, Avilés, Spain, and in part by the Ministry of Economy and Competitiveness of Spain (project within the framework of the National Plan of Research, Development and Innovation, reference ENE2014-52272-R).

G. A. Orcajo, J. Rodríguez D., J. M. Cano, and J. G. Norniella are with the Department of Electrical Engineering, University of Oviedo, 33204 Gijón, Spain (e-mail: gonzalo@uniovi.es; josue.rodriguez.diez@cern.ch; jmcano@uniovi.es; jgnorniella@uniovi.es).

P. Ardura G., R. Llera T., and D. Cifrián R. are with the Department of Global Research and Development, ArcelorMittal, 33400 Avilés, Spain (e-mail: pablo.ardura@arcelormittal.com; rocio.llera@arcelormittal.com; diego.cifrian@arcelormittal.com).

Color versions of one or more of the figures in this paper are available online at http://ieeexplore.ieee.org.

Digital Object Identifier 10.1109/TIA.2016.2533483

A large part of the steel production costs is due to energy usage. Savings can be achieved by producing in a more efficient way. Furthermore, more energy-efficient production processes lead to a reduction in the environmental impact. Therefore, it is useful to identify the energy usage of the production process and also the quality of energy.

Energy is considered to be strategic for the iron- and steelmaking sectors. Energy typically represents 15%–20% of the operating costs of a steel plant, and has also direct implications for greenhouse gas regulatory compliance costs. hot rolling operation represents approximately 8% of the total energy consumption in an integrated steelworks. Hot rolling is the process with the largest electrical energy demand, accounting for 20% of the total consumption (approximately 80 kWh/ton), and one of the most critical ones in terms of power quality. Not only is the average load considerable, but the dynamic load variation is also large because the mill repeatedly runs through its process cycle [1].

The aim of this paper is to obtain a better understanding of electric energy usage in the hot rolling operation and to define and validate major opportunities for daily energy predictions.

### A. Short-Time Prediction of Electrical Demand and Power-Quality Parameters

It is crucial to estimate the power demand of a steel plant both in the design stage and under different operating conditions. Estimation allows for guaranteeing the ability of the plant to withstand the anticipated load, calculating the nominal capacity of the lines, designing the protections, etc. Hybrid solutions for filtering and compensating for reactive power are becoming more common in this type of facilities. Such an ad hoc design requires a thorough analysis of reactive power variations and a study of the planned injection of harmonics into the network. Moreover, the aforementioned estimation is necessary to ensure the stability of the voltage at the point of common coupling, the electromagnetic compatibility of the system with the network, the minimization of operation losses, and the elimination of penalties from utilities [3].

Most of the electrical variables that characterize power quality and the electromagnetic compatibility of a hot rolling mill are related to the particular rolling conditions at the instant of analysis. Considering the high order of magnitude of the driven power and the strongly nonlinear characteristic of the load (Fig. 1), the variability of the conditions has a great impact on the main representative parameters of power quality.

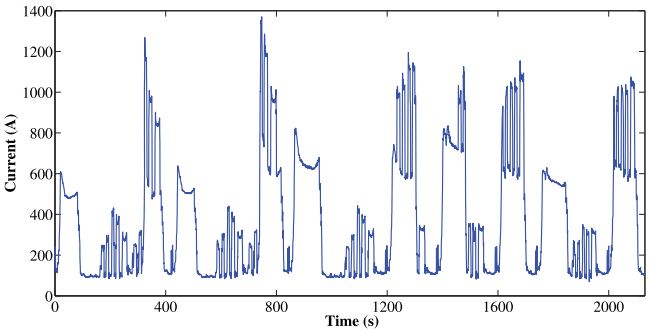


Fig. 1. Evolution of measured line current rms value during coil rolling.

These electrical magnitudes are highly dependent on the rolling-process conditions, the chemical composition of the steel slab, and the mechanical characteristics that the final coil is intended to have. Hence, the interest in developing an analytical method capable of reproducing the particular operating conditions of a hot rolling mill and predicting the evolution of the main electrical variables that are involved.

### *B. Daily Prediction of Hot Strip Mill Consumption*

Daily prediction of large facilities' consumption allows for significant savings in the cost of electricity. If the energy market liberalization is taken into account, a prediction can be leveraged to improve the negotiation with the utility and obtain more competitive prices in the electricity market.

Therefore, it is crucial to monitor and record (e.g., by using a SCADA system) the electrical variables of the process along with its key operating parameters to predict their influence on the electrical consumption.

However, the high variability of the operating conditions of the process can hamper the drawing of conclusions regarding the independent influence of each variable. Therefore, models that reproduce the operation of the facility as closely as possible are advisable. Such models should be compared to actual variables and validated afterward. Once validated, the models become an important source of information to identify trends in consumption. These trends can be analyzed by varying a selection of influential variables; such a study is very complicated when conducted just on the basis of field measurements.

## II. Hot Rolling Mill

### *A. Roughing and Finishing Mills*

The modeled hot rolling mill is a classic facility mainly comprising one roughing and six finishing mill stands (Fig. 2). The behavior of additional equipment such as coiling machines, edgers, and crop shear has not been reproduced in the model because the major consumption of electricity is associated with the roughing and finishing mills.

The roughing mill consists of two stands, one at the top side and the other one at the bottom side. The drives are circulating-current-free and double-cascade-connected cycloconverters. The double-cascade configuration allows for a better power factor by means of asymmetric and bias voltage control. The rated data for the main equipment are shown in Table I.

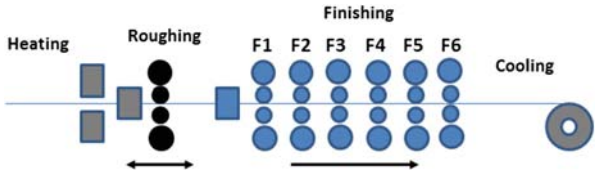


Fig. 2. Schematic of the rolling-mill train.

TABLE I
Main Characteristics of the Stands

| Stands | Motor power (MW) | Poles | Cycloconverter | Transformer power (MVA) |
|---|---|---|---|---|
| F1 | 8.0 | 6 | Circulating-current-free | 14.4 |
| F2 | 8.0 | 6 | Circulating-current-free | 14.4 |
| F3 | 8.0 | 6 | Circulating-current-free | 14.4 |
| F4 | 8.0 | 6 | Circulating-current-mode | 15.7 |
| F5 | 8.0 | 6 | Circulating-current-mode | 15.7 |
| F6 | 8.0 | 6 | Circulating-current-mode | 15.7 |
| Top roughing | 7.5 | 12 | Circulating-current-free | 14.4 |
| Bottom roughing | 7.5 | 12 | Circulating-current-free | 14.4 |

The finishing mill consists of six stands, three of them (F1, F2, and F3) being driven by means of circulating-current-free, double-cascade-connected, 12-pulse three-phase cycloconverters. The other stands (F4, F5, and F6) are driven from circulating-current-mode, 12-pulse three-phase cycloconverters.

Circulating-current control allows for the increase in the demand of reactive power when the plant operates at low load.

Since the 1970s, synchronous motors fed by thyristor-based cycloconverters controlled by field-oriented control (FOC) have been extensively used in hot rolling mills. Since the 1980s, the trends in steel mill drives have been to use pulsewidth modulation (PWM)-based voltage source inverters (VSI). Despite the technological improvement that the use of inverters involved, in the 1990s, up to 10 hot rolling mill lines based on cycloconverters were installed. This technology is used today by many rolling-mill plants [4], [5].

The development of new high-power semiconductors and multilevel inverter topologies has led to an increased application of PWM-controlled VSI ranging from 0.5 MVA to approximately 30 MVA. Converters for steel mill drives must achieve good dynamic properties and a low torque ripple, control reactive power consumption, and harmonic current injection, and be characterized by a high efficiency and adjusted complexity and dimensions. In addition to the application of FOC in inverter-fed motor drives with various PWM schemes, such as carrier-based, hysteresis band control and space vector modulation, the recent application of direct torque control (DTC) to ac drives in plate rolling mills has been claimed as achieving the highest torque and speed performance ever attained with variable speed drives, making it possible to control the full torque within a few milliseconds and reduce the impact of load shocks.

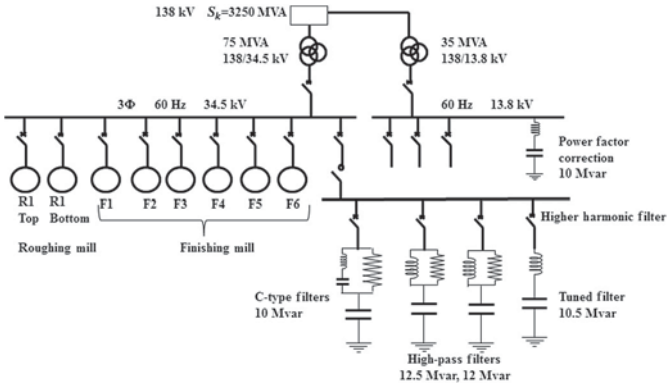


Fig. 3. Single-line diagram distribution network and filtering system.

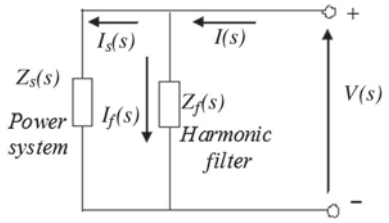


Fig. 4. Current divider based on the filter/system impedance.

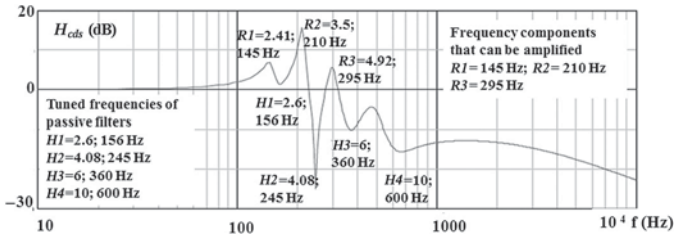


Fig. 5. Frequency response of $H_{cds}(s)$.

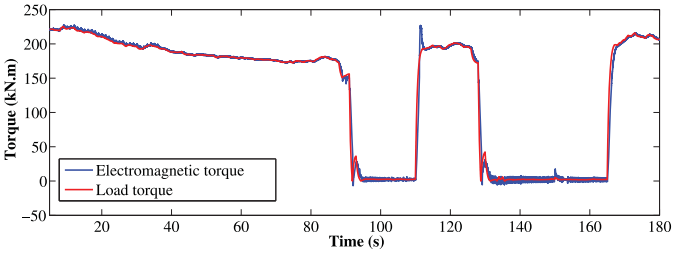


Fig. 6. Calculated electromagnetic torque versus measured load torque in stand F2.

### B. Distribution Network Topology and Filtering System

The hot rolling mill is connected to a 138-kV, 60-Hz, 3600-MVA power distribution network through a 75-MVA, 138/34.5-kV transformer. The eight stands of the hot rolling mill are fed from a 34.5-kV bus. Four banks of passive filtering are also connected to these same bars. The filtering system comprises one C-filter, two second-order high-pass filters, and one tuned filter. The global passive filter enables the compensation for 45 Mvar at 34.5 kV (Fig. 3). The passive harmonic filter has been designed to improve the harmonic response and provide the reactive-power compensation [6].

As shown in Fig. 4, $H_{\text{cds}}(s)$ is the transfer function of a current-divider that considers the relationship between the power system current $I_s$ and the current injected from the load $I$

$$H_{\text{cds}}(s) = \frac{I_s(s)}{I(s)} = \frac{Z_f(s)}{Z_f(s) + Z_s(s)}. \tag{1}$$

Fig. 5 shows the attenuation provided by the filtering system in coordination with the impedance of the power distribution system. The transfer function $H_{\text{cds}}(s)$ is based on the single-phase equivalent circuit assuming that the system is balanced [7]. The attenuation factor of the filter bank is mainly effective for high frequencies. Therefore, although high-frequency components are attenuated, some interharmonics on the low-frequency side are still present and, in some cases, could be amplified due to parallel resonances.

## III. Analysis Method

The developed analysis method is aimed to identify the key variables influencing the electrical behavior of the main stands of a hot rolling-mill plant. This process is based on both the characteristics of the steel to be milled and the particular features of the rolling mill. The method provides the evolution of the main electrical variables that are involved.

The demand of active and reactive energy, the consumption of active and reactive power, and the current harmonic injection into the power distribution system are the main variables of interest to be calculated. The results have been compared to the corresponding measurements in an actual rolling plant and then validated.

The main stands of the mill, the power network, and the filter banks have been modeled by using a program for simulating electrical power systems [8]. Each stand has been modeled by including a 33/1.15-kV step-down transformer, which converts the 6-pulse topologies of the individual rectifiers to 12-pulse cycloconverter topologies. Each stand includes six transformers (two transformers per phase). Cycloconverters with their corresponding control stage have also been modeled [9] (bias control, asymmetrical control, circulating current control, etc.), as well as the synchronous motor vector control that determines the modulation index and the phase angle of the control signal.

The load torque developed by the rollers of each stand is applied to the motor (Fig. 6). The control system uses the speed as a reference (Fig. 7). Both variables are subject to the necessary adaptations to the speed-reducer gearboxes and the consequent performance ratio. Therefore, torque and speed are the inputs to the developed electric model.

The FOC method is used to control the synchronous motor [10]. This strategy pursues the decoupling of flux and torque control. Therefore, the flux can be mostly fixed by the field windings, while the armature current is used to achieve the motor torque. The motor torque is set through a speed control loop that tracks the speed reference and takes the load torque as a disturbance. All of the main loops of the FOC method have been modeled (Park transformations, flux observer, armature current, field current and speed loops). There are three different control loops.

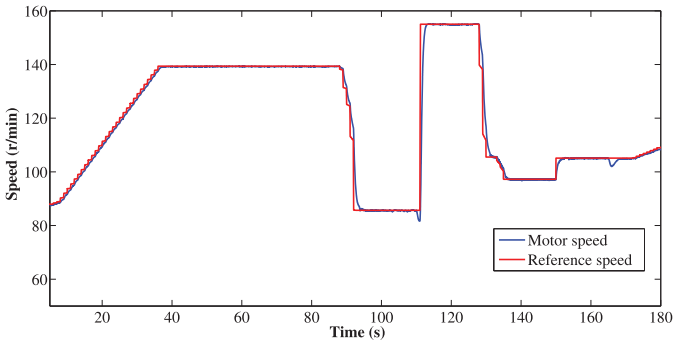


Fig. 7. Speed control in stand F2; calculated motor speed versus measured reference speed.

1) Speed loop: To set the flux and motor torque references after tracking the speed reference and performing the field weakening.
2) Flux loop: To estimate the flux position through an observer and control the field current.
3) Current loop: To track the armature current components (mostly torque current).

The cycloconverter firing signal generator has also been modeled. The voltage reference set by the motor control and the currents are the inputs of the generator and are used for the inhibition of the current-free cycloconverter firing pulses.

Furthermore, the generator uses the cosine-wave crossing technique for the gate signal generation and other secondary control techniques for enhancing the reactive-power consumption. Such control techniques are as follows.

1) Asymmetric control is a strategy used in cascade cycloconverters based on the nonidentical firing signals between the two series-connected bridges. The effect is an asymmetric firing in the cascade bridges. It has been implemented in the circulating-free-current cycloconverters (R1, R2, F1, F2, and F3).
2) Reactive control through circulating current aims to consume a higher reactive current in the circulating-current-mode cycloconverters (F4, F5, and F6) when the overall reactive consumption of the plant is low (e.g., in the standstills) and the filters overcompensate for the reactive power.
3) Bias control aims to achieve voltages with higher rms values at the converter output through third harmonic injection. This kind of control leads to a higher voltage level feeding the motor and, therefore, a decrease in the input reactive power.

## IV. Types of Steel, Chemical, and Alloy Composition

Three grades of steel with different carbon content are considered, thus involving different hardness characteristics. Steel types "A," "B," and "C" have low, medium, and high carbon content, respectively. Characteristics of steel are documented in AISI/SAE standard (American Iron and Steel Institute / Society of Automotive Engineers). The chemical composition of each type of steel and its physical and mechanical properties can be obtained from the aforementioned standard (Tables II and III).

TABLE II
Chemical Composition of the Three Types of Steel

| Element | Steel A-content (%) | Steel B-content (%) | Steel C-content (%) |
|---|---|---|---|
| Iron | 99.3–99.7 | 99.16–99.6 | 98.46–98.92 |
| Manganese | $\leq 0.6$ | 0.3–0.6 | 0.6–0.9 |
| Carbon | $\leq 0.12$ | 0.1–0.15 | 0.47–0.55 |
| Sulfur | $\leq 0.045$ | $\leq 0.05$ | $\leq 0.05$ |
| Phosphorous | $\leq 0.045$ | $\leq 0.04$ | $\leq 0.04$ |

TABLE III
Mechanical Properties of the Three Types of Steel

| Properties | Steel A | Steel B | Steel C |
|---|---|---|---|
| Tensile strength (MPa) | 325 | 370 | 690 |
| Yield strength (MPa) | $\geq 280$ | 310 | 580 |
| Elastic modulus (GPa) | 210 | 190–210 | 190–210 |
| Poisson´s ratio | 0.27–0.3 | 0.27–0.3 | 0.27–0.3 |
| Elongation at break (%) | 28 (in 80 mm) | 19 (in 50 mm) | 10 (in 50 mm) |
| Hardness, vickers | 105 | 108 | 207 |
| Density (g/cm$^3$) | 7.872 | 7.87 | 7.85 |

Standard SAE J403 1010 [11] is used for type "A" steel and Standard SAE J403 1012 [12] for type "B" steel. The SAE standards between 1005 and 1015 are used for steel whose carbon content is between 0.06% and 0.18%. Standard SAE J403 1050 [13] is used for type "C" steel. SAE standards between 1035 and 1053 are used for steel whose carbon content is between 0.32% and 0.55%.

## V. Mill Process: Influencing Variables

The slab reaches the roughing mill free of mill scale, where it is given the correct thickness to enter the finishing mill train. Five to seven passes are run in the four-high reversing stand to roll the slab down to the required transfer-bar thickness. The number of passes depends on the measurements of the slab, the steel plate to be obtained, the grade of steel, and the final rolling temperature in the train. The steel plate leaving the roughing mill train is subject to a single pass in the continuous finishing train, then partially cooled but coiled while still hot. The finishing mill train consists of six nonreversible two-high arrangement stands where the required final thickness is achieved. The temperature varies between $800\,^{\circ}\mathrm{C}$ and $1250\,^{\circ}\mathrm{C}$. Hot rolling must be conducted at the appropriate temperature, both on the surface and inside the material [14], [15].

For the determination of the mechanical conditions of the rolling mill, mathematical models able to interrelate the process variables with the characteristics of the steel sheet are used. The models provide data about reductions in stands, roll speeds, temperature at the end of the last stand, cooling rate, coiling temperature, etc. Several programs allow for estimating the rolling conditions, such as StripCam and HSMM (Hot Strip Mill Model). Both programs are capable of interrelating the rolling-process variables with the mechanical properties of the steel to be obtained [15], [16].

## VI. Synchronous Motors Load Torque and Speed

Rolling conditions for each type of steel are described as follows. The required load torque and speed of the motors are calculated from the following summarized conditions.

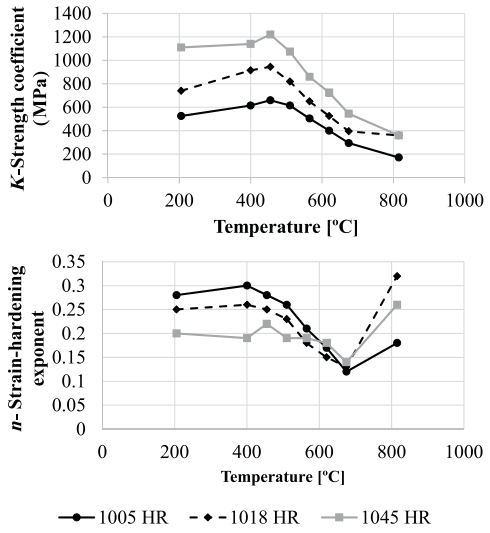


Fig. 8. Typical values of $K$ and $n$ for different types of hot rolled steel [18].

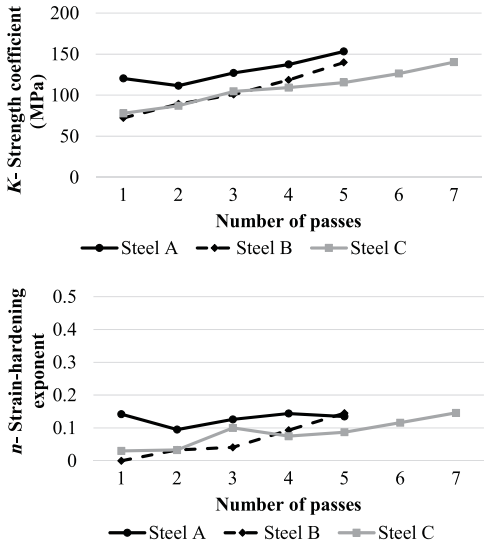


Fig. 9. Top: $K$-strength coefficient. Bottom: $n$-strain hardening exponent.

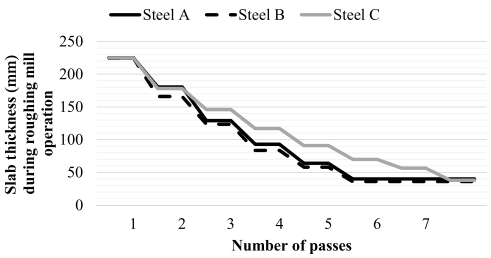


Fig. 10. Calculated thickness of the slab during the passes in roughing mill.

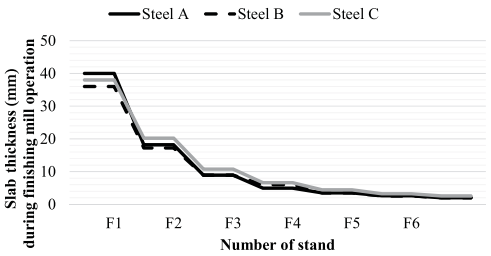


Fig. 11. Calculated thickness of the slab during the passes in finishing mill.

### A. Flat Rolling

In flat rolling [17], the thickness is reduced by an amount called the draft

$$d = t_0 - t_f \tag{2}$$

where $d$ is the draft, $t_0$ is the starting thickness, and $t_f$ is the final thickness.When selecting the draft, it is necessary to optimize the mill operation within the limits set by the rated power of the motors. The true strain $\epsilon$ undergone by the work in rolling depends on the previous and subsequent stock thicknesses

$$\varepsilon = \ln \frac{t_0}{t_f}. \tag{3}$$

The average flow stress $\overline{Y_f}$, applied to the work material in flat rolling, is determined from the true strain

$$\overline{Y_f} = \frac{K \cdot \varepsilon^n}{1+n}. \tag{4}$$

Values of the strength coefficient $K$ and the strain-hardening exponent $n$ depend on the composition, the heat treatment, and the work hardening. The higher the carbon content is, the higher the strength coefficient results (Fig. 8). The average flow stress is used to estimate the rolling force and power.

An approximation of the rolling force $F$ can be calculated from the average flow stress

$$F = \overline{Y_f} \cdot w \cdot L \tag{5}$$

where $w$ is the material width and $L$ is the contact length, which considering $R$ the roll radius is approximately

$$L = \sqrt{R \cdot (t_0 - t_f)}. \tag{6}$$

The power $P$ required to drive two powered rolls is twice as much as the product of the torque for each roll and the angular velocity. The torque for each roll $T$ is

$$T = 0.5 \cdot F \cdot L \tag{7}$$

and the active power is

$$P = F \cdot L \cdot \omega_r \tag{8}$$

where $\omega_r$ is the rotational speed in radians per second. The active power demanded by the motors must be correctly distributed by choosing the strip thickness at the delivery side of each stand. Temperature and deformation resistance play an important role in the distribution of forces in the stands.

### B. Steel Types: Rolling Conditions

The behavior of the three types of steel has been obtained from their chemical composition (see Table II). Fig. 9 shows $K$-strength coefficient and $n$-strain-hardening exponent at the rolling temperature during the corresponding passes. The strip thickness at the delivery side of each stand has been chosen (Figs. 10 and 11) by considering the constraints on the power

TABLE IV
GEOMETRY OF THE SLAB FOR DIFFERENT TYPES OF STEEL

| Element | Steel A | Steel B | Steel C |
|---|---|---|---|
| Slab length (m) | 10 | 11 | 11 |
| Slab width (mm) | 1259 | 1224 | 1248 |
| Slab weight (ton) | 22.75 | 23.78 | 24.68 |

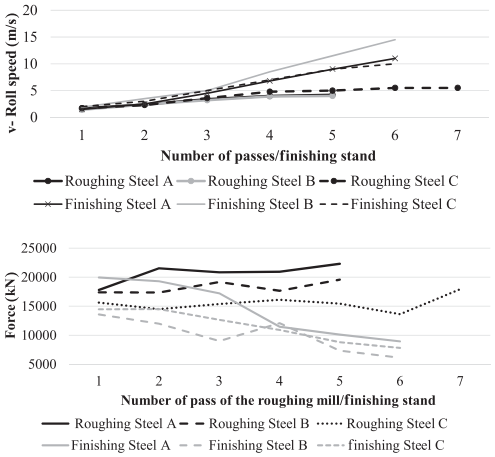


Fig. 12. Top: calculated roll speed during the rolling of steel types A, B, and C. Bottom: calculated rolling force during steel mill.

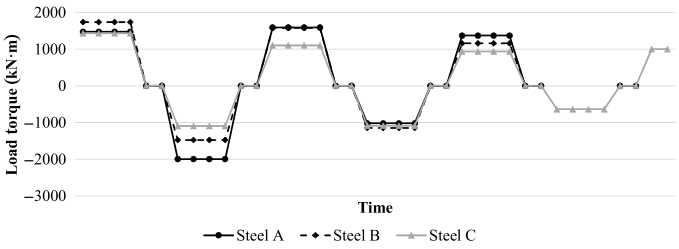


Fig. 13. Calculated load torque of the roughing mill stands during milling of different types of steel.

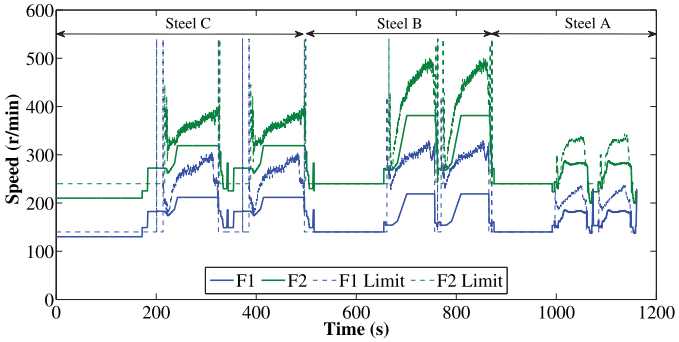


Fig. 14. Speed limits of stands F1 and F2 versus selected and calculated speed.

and speed of the stands and the measurements of the slab and the rolls (Table IV).

The average flow stress is obtained from (4) and, then, the force and torque applied by each roller are calculated from (5) and (7). Constraints to the speed/frequency and maximum power at the stands must be considered to set the speed of the rolls. The mechanical conditions in Figs. 12 and 13 correspond to rolls' data. Speed limits for stands F1 and F2 are observed

TABLE V
VALIDATION OF THE TENSILE STRENGTH FROM SIMULATION

| Tensile strength | Steel A | Steel B | Steel C |
|---|---|---|---|
| Simulation (MPa) | 355 | 352 | 661 |
| Standard (MPa) | 325 | 370 | 690 |

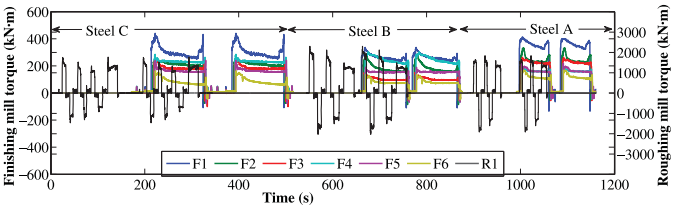


Fig. 15. Measured load torque at the stands during steel milling.

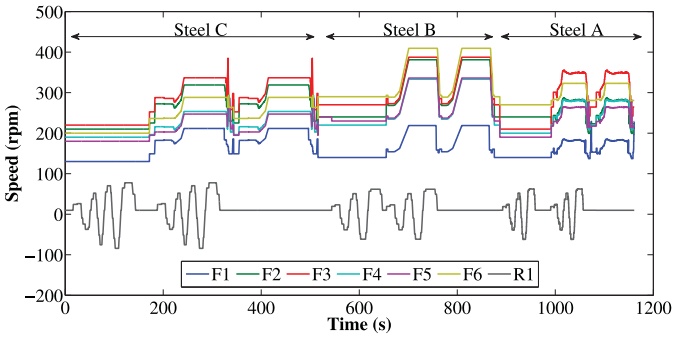


Fig. 16. Measured motor speed in the stands of the rolling mill during steel milling.

in Fig. 14. These stands are subject to higher torques in the finishing mill and, therefore, the constraints on speed are more severe. The tensile strength obtained from the estimation of the mechanical rolling conditions is compared to that provided by the standard (Table V).

Estimation is validated because the values of the tensile strength have the same order of magnitude. The evolution of the load torque and the motor speed at the stands of the roughing and finishing mill drives, corresponding to motor conditions, are shown in Figs. 15 and 16. In the case of the finishing mill, the ratios of the gearboxes incorporated into the stands must be considered: $F1 = 5.2$; $F2 = 4.5$; $F3 = 3.0$; $F4 = 1.478$: $F5 = 1.0$; and $F6 = 1.0$. The roughing mill does not incorporate any gearboxes.

## VII. POWER AND ENERGY DEMAND

The demanded active power is directly calculated from the values of the torque and speed of the rolling-mill motors, the performance ratio of the drives and the transformer, and stand-line losses. Reactive-power values are mainly obtained from the cycloconverter mean trigger angle (Fig. 17). All represented records in this section have been calculated. The analysis procedure has been validated in Section VIII using on-site measurements. This angle depends on the load angle $\phi_0$ and the cycloconverter modulation index $m$. The relationship among

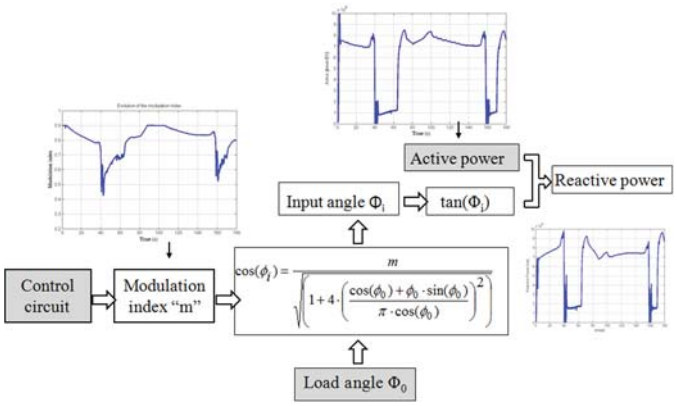


Fig. 17. Flow diagram for calculating reactive-power consumption.

the load angle, the modulation index, and the displacement factor at the input $\cos(\Phi_i)$ is as follows [19]:

$$\cos(\Phi_i) = \frac{m}{\sqrt{\left(1 + 4 \times \left(\frac{\cos(\Phi_0) + \Phi_0 \cdot \sin(\Phi_0)}{\pi \cdot \cos(\Phi_0)}\right)^2\right)}}. \quad (9)$$

In the case of synchronous motors fed from the cycloconverters, the output displacement factor is close to unity because vector control forces the synchronous motor to operate with unity power factor. The highest input displacement factor is reached when the output voltage is maximum and, therefore, the modulation index is equal to 1 [20], [21]. At low-modulation index operation (low load), higher values of reactive power are absorbed by the cycloconverter, whereas the active power absorbed by the cycloconverter increases and the reactive power decreases with a high modulation index [22]. The reactive power $Q$ is estimated from the active power and the input displacement factor

$$Q = P \cdot \tan(\Phi_i). \quad (10)$$

The reactive-power demand in stands F4, F5, and F6 is controlled by the active control of reactive power [23], [24]. Overcompensation in the distribution network is avoided at low-load intervals because the extra reactive power from the filter banks is demanded by these stands. These stands are forced to consume an extra reactive power $Q_0$ to compensate for the reactive power injection from the filter banks. $Q_0$ is calculated by subtracting the reactive power injected by the different filter banks and the reactive power consumed by the stands, which is associated with the particular loading conditions. Such a difference is divided by 3 when positive in order to distribute it among the three stands with circulatory current. Each stand will provide a maximum value of reactive power depending on the maximum power that the converter can drive and the active and reactive power associated with the loading conditions.

Fig. 18 shows four kinds of reactive power: the reactive power associated with the particular loading conditions, the maximum reactive power that the drive can deliver through the circulating current, the reactive power consumption associated with the circulating current, and the final demand of reactive power associated with stand F4.

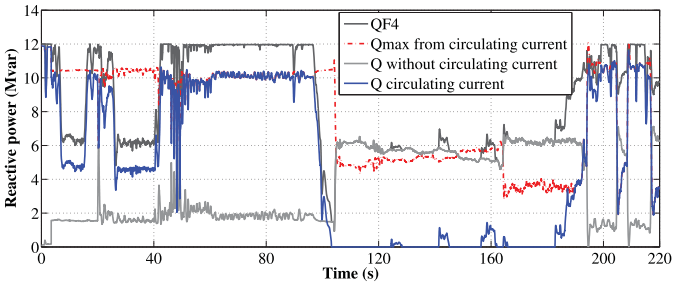


Fig. 18. Evolution of reactive-power demands at stand F4.

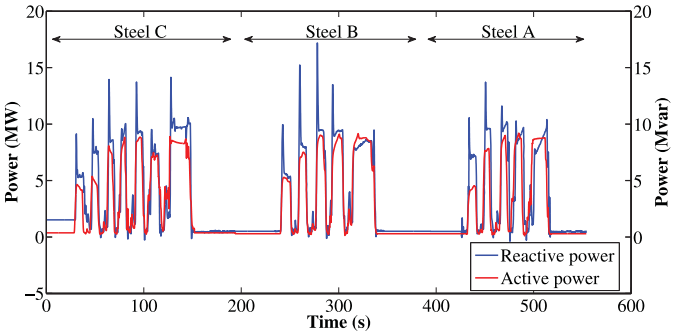


Fig. 19. Active and reactive power demanded by top roughing-mill drive.

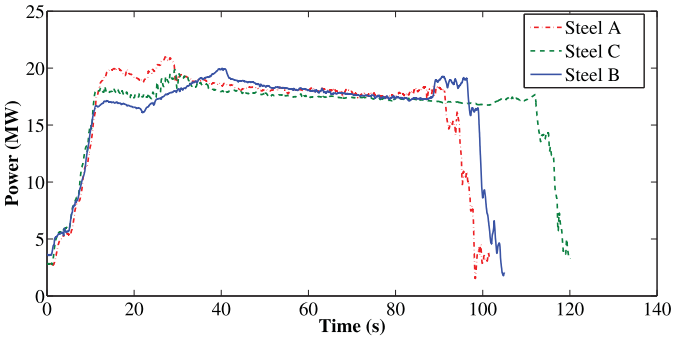


Fig. 20. Active power demanded by the finishing mill.

### A. Roughing Mill

In this section, a comparative analysis of the active and reactive power consumption in the roughing mill has been performed (Fig. 19). Type-C steel requires seven passes.

Steel types A and B require only five passes. The maximum consumption is limited by the maximum power that the drives can deliver. Both active and reactive energies increase with the steel hardness. The demand of active energy for type-C steel is 39% greater than that required for type-A steel.

### B. Finishing Mill

The study conducted for the roughing mill is also performed for the finishing mill train (Fig. 20). In this case, the maximum values of active-power demand have the same order of magnitude and the difference between the types of steel relies on the duration of the mill period. Fig. 19 shows a difference of 20 s over a maximum period of 120 s.

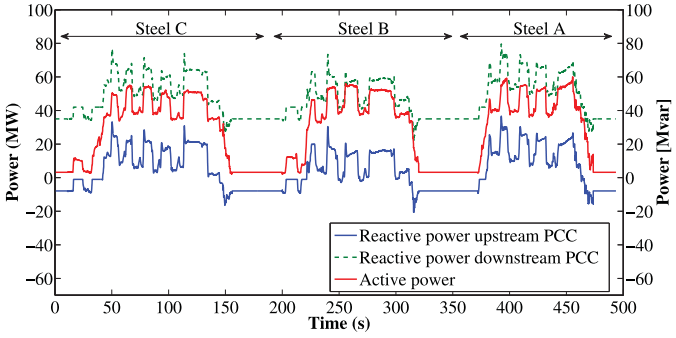


Fig. 21. Active and reactive power demanded by hot rolling mill.

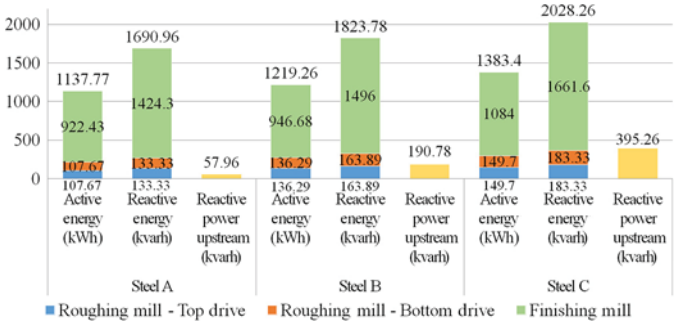


Fig. 22. Active and reactive energy demanded by hot rolling mill.

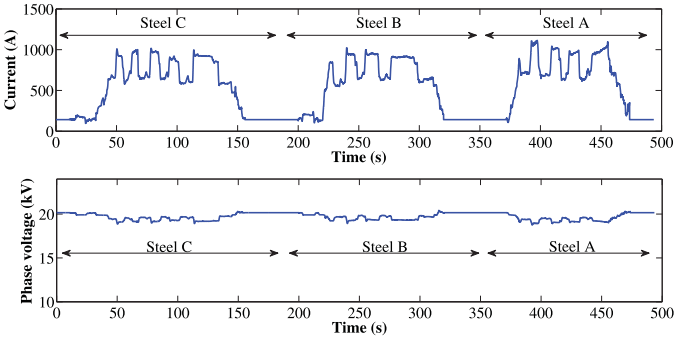


Fig. 23. Evolution of the rms value of the current upstream of the PCC and of the phase voltage at the PCC.

## C. Global Demand

Possible overlapping of roughing and finishing mill trains must be considered for a global analysis of the demand. When overlapping does not occur, the consumption is sequential and the demands of active and reactive power are those corresponding to these trains, although not synchronized.

Fig. 21 shows that the active and reactive powers flow downstream and upstream of the point of common coupling PCC. These variables are used to estimate the energy demand (Fig. 22) and the evolution of the rms value of the current and voltage (Fig. 23). Knowledge of the evolution of the rms value of the voltage at the coupling point is crucial to ensure compliance with the requirements set by standards [25].

The frequency components of the currents demanded by the stands are dependent on the number of converter pulses and the output frequency of the cycloconverter, and, the motor speed. The amplitudes and phase angles of these components are quantities that depend fundamentally on the analyzed

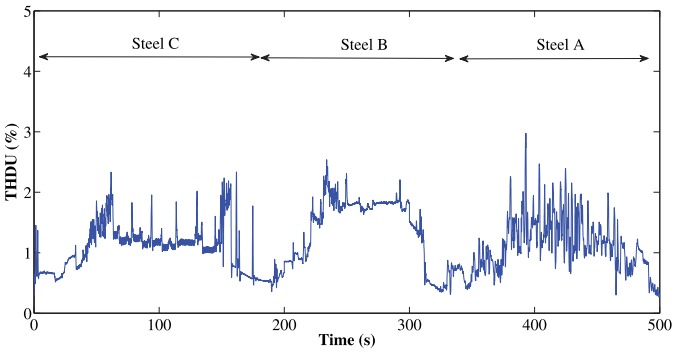


Fig. 24. Evolution of the voltage THD at the PCC.

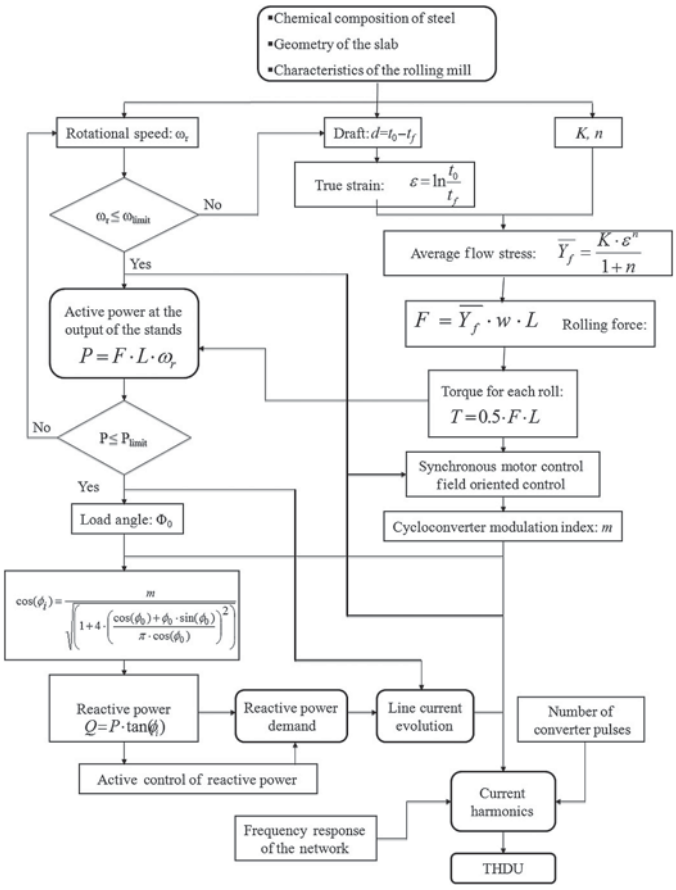


Fig. 25. Simplified flowchart to estimate the main variables.

frequency, the modulation index of the cycloconverter, and the filtering inductive impedances of the circuits [21].

The frequency components from the stands, along with the frequency response of the filter stage and the distribution network (Fig. 5), allow for performing the analysis of the dynamic evolution of the total harmonic distortion (THD) of the voltage at the coupling point (Fig. 24).

## VIII. Validation of the Results

The validation of the electric model is demonstrated by comparing its results with on-site measurements during the rolling of type "A" steel. To obtain the calculated variables, the rolling process is simulated and the main variables are estimated according to the flowchart shown in Fig. 25 [26]. The

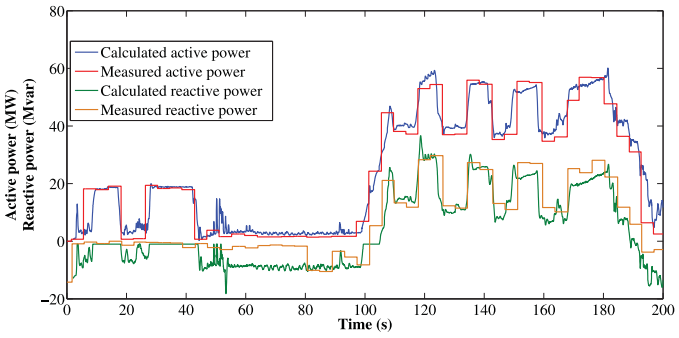


Fig. 26. Validation of active and reactive power demanded by rolling mill.

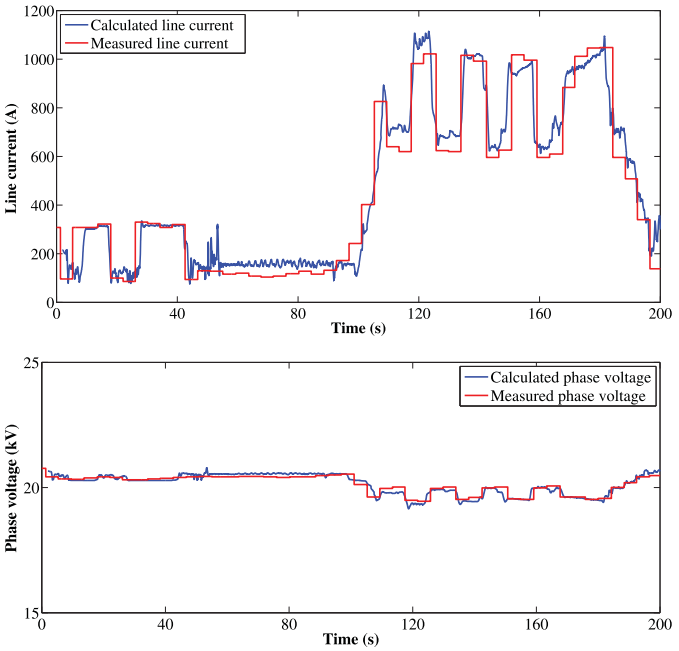


Fig. 27. Validation of the rms value of the current upstream of the PCC and of the phase voltage at the PCC.

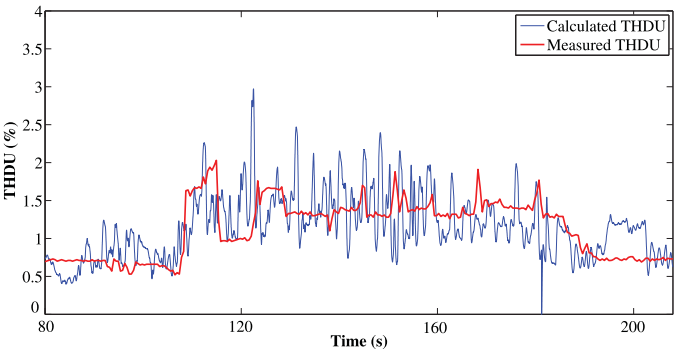


Fig. 28. Validation of the voltage THD at the PCC.

evolution of the main electrical variables for the same type of steel is shown in Figs. 26–28, which is obtained from on-site measurements, and is compared with the similar evolution of the calculated variables.

The sampling frequency is 25 kHz for the calculated variables and 100 Hz for the measured variables. The measured THD of the voltage is a time-averaged record, whereas the calculated THD has been obtained at a higher registering frequency. Because torque and speed, which feed the model, experience a significant change in the process that is reproduced, the electrical variables also experience significant dynamic variations.

The achieved adjustment as shown in the Figs. 26–28 is accurate. The major discrepancies occur at periods of low load, due to the fact that only the most significant loads have been modeled (finishing and roughing mill) and the impact of these discrepancies is not relevant to the overall analysis.

## IX. Conclusion

The relationship among the properties of the steel to be milled, the mechanical conditions of the rolling mill, the technical features of the roughing and finishing mills, and the involved electrical variables has been obtained. The proposed method provides a powerful analytical tool for the prediction of the electrical demand and the power-quality parameters. The continuous variability of the process operating conditions can hinder the drawing of conclusions from actual measurements regarding the independent influence of each variable.

A complete hot-strip-mill facility has been modeled. Each stand of the roughing and finishing mills has been simulated. The electric distribution system of the factory with the existing passive filtering stage has been modeled as well. The model has been tested with several load profiles by using the torque and speed variables as input data, and with on-site measurements of voltage, current, active and reactive power, torque, and rolling speed. A database with three steel types has been analyzed, which allows for correlating the type of steel with the electrical demand and several power-quality parameters. A simple algorithm has been developed to set a correlation between the mill operation conditions and the electrical demand of the facility. The influence of several mechanical variables and electrical variables on power demand and power quality has been analyzed.

## References

[1] E. Kun and T. Szemmelveisz, "Energy efficiency enhancement in the Hot Rolling Mill," *Mater. Sci. Eng.*, vol. 3, no. 2, pp. 43–50, 2014.

[2] University of Oviedo, Arcelormittal Spain, Centre de Recherches Metallurgiques ASBL, Vdeh-Betriebsforschungsinstitut Gmbh, "Minimising energy loss in hot rolling by intelligent manufacturing," Eur. Comm., Res. Fund Coal Steel, Directorate-General Res. Innov., Eur. Comm., Brussels, Belgium, Tech Rep. UE-10-RFSR-CT-2010-00008, Dec. 2013.

[3] C. S. Chen, Y. D. Lee, C. T. Hsu, D. S. Ting, and C. C. Shen, "Power quality assessment of a hot strip mill with cycloconverter drive systems," in *Proc. 42nd IEEE IAS Annu. Meeting*, New Orleans, LA, USA, Sep. 2007, pp. 9–16.

[4] H. Hosoda, S. Kodama, and R. Tessendorf, "Large PWM inverters for rolling mills," Assoc. Iron Steel Technol., Warrendale, PA, USA, PR-PM0108-4, Jan. 2008.

[5] A. K. Chattopadhyay, "Alternating current drives in the steel industry, advancements in the last 30 years," *IEEE Ind. Electron. Mag.*, vol. 4, no. 4, pp. 30–42, Dec. 2010.

[6] A. B. Nassif and W. Xu, "Passive harmonic filters for medium-voltage industrial systems: Practical considerations and topology analysis," in *Proc. 39th North Amer. Power Symp. (NAPS)*, Las Cruces, NM, USA, Sep. 2007, pp. 301–307.

[7] J. K. Phipps "A transfer function approach to harmonic filter design," *IEEE Ind. Appl. Mag.*, vol. 38, no. 2, pp. 68–82, Mar./Apr. 1997.

[8] MathWorks. (2010). *The MathWorks—MATLAB and Simulink for Technical Computing* [Online]. Available: http://www.mathworks.com

[9] W. Timpe, "Cycloconverter drives for Rolling Mills," *IEEE Trans. Ind. Appl.*, vol. IA-18, no. 4, pp. 400–404, Jul./Aug. 1982.

[10] J. R. Rodríguez *et al.*, "Technical evaluation and practical experience of high-power grinding mill drives in mining applications," *IEEE Trans. Ind. Appl.*, vol. 41, no. 3, pp. 866–873, May/Jun. 2005.
[11] *Chemical Compositions of SAE Carbon Steels*, AISI/ASE Standard, SAE J403 1010, Jun. 2014.
[12] *Chemical Compositions of SAE Carbon Steels*, AISI/ASE Standard, SAE J403 1012, Jun. 2014.
[13] *Chemical Compositions of SAE Carbon Steels*, AISI/ASE Standard, SAE J403 1050, Jun. 2014.
[14] J. L. E. Berciano, E. T. Guerra, S. E. de Bengy, and D. F. Segovia, *Laminación. Monografías sobre Tecnología del Acero. IV*. Madrid, Spain: UPM Tech. Univ. Madrid, Jan. 2010, pp. 36–49.
[15] F. Yamada *et al.*, "Hot Strip Mill mathematical models and set-up calculation," *IEEE Trans. Ind. Appl.*, vol. 27, no. 1, pp. 131–139, Jan./Feb. 1991.
[16] U. Lotter, H.-P. Schmitz, and L. Zhang, "Application of the metallurgically oriented simulation system "TKS-StripCam" to predict the properties of Hot Strip Steels from the rolling conditions," *Adv. Eng. Mater.*, vol. 4, no. 4, pp. 207–213, Apr. 2002.
[17] M. P. Groover, *Fundamentals of Modern Manufacturing. Materials, Processes and Systems*, 4th ed. Hoboken, NJ, USA: Wiley, 2010, pp. 395–403.
[18] J. R. Davis, S. L. Semiatin, and American Society for Metals, *ASM Handbook, vol. 14, Forming and Forging*. Materials Park, OH, USA: ASM International, 1996, pp. 351–355.
[19] J. M. D. Murphy and F. G. Turnbull, *Power Electronic Control of AC Motors*. New York, NY, USA: Pergamon, 1989, pp. 199–216.
[20] P. Aravena, L. Morán, J. Dixon, J. Espinoza, and O. Godoy, "A new hybrid filter topology for sub and inter-harmonic attenuation in cycloconverter-fed drives applications," in *Proc. IEEE IAS Ind. Appl. Soc. Annu. Meeting*, Houston, TX, USA, Oct. 4–8, 2009, pp. 1–7.
[21] B. R. Pelly, *Thyristor Phase-Controlled Converters and Cycloconverters*. Hoboken, NJ, USA: Wiley, 1971.
[22] P. Aravena, L. Morán, R. Burgos, P. Astudillo, C. Olivares, and D. A. Melo, "High-power cycloconverter for mining applications: Practical recommendations for operation, protection, and compensation," *IEEE Trans. Ind. Appl.*, vol. 51, no. 1, pp. 82–91, Jan./Feb. 2015.
[23] S. G. Bosga, J. L. Duarte, and A. J. Vandenput, "Natural circulating current control of a cycloconverter," in *Conf. Rec. IEEE Ind. Appl. Soc. Annu. Meeting*, Toronto, ON, Canada, Oct. 1993, vol. 2, pp. 1160–1165.
[24] S. Tanaka, "Control method for cycloconverter and control apparatus therefor," U.S. Patent 4 670 826, Jun. 2, 1987.
[25] *IEEE Recommended Practices and Requirements for Harmonic Control in Electrical Power Systems*, IEEE Standard 519-2014, 2014.
[26] G. A. Orcajo *et al.*, "Dynamic estimation of electrical demand in hot rolling mills," in *Proc. IEEE Ind. Appl. Soc. Annu. Meeting*, Dallas, TX, USA, Oct. 18–22, 2015, pp. 1–9.

**Gonzalo Alonso Orcajo** was born in Gijón, Spain, in 1965. He received the M.Sc. and Ph.D. degrees in electrical engineering from the University of Oviedo, Gijón, Spain, in 1990 and 1998, respectively.

In 1992, he joined the Department of Electrical Engineering, University of Oviedo, where he is currently an Associate Professor. His research interests include power quality in industrial power systems, detection and location of faults in distribution systems, and reactive power compensation systems.

**Josué Rodríguez D.** was born in Pravia, Spain, in 1989. He received the M.Sc. degree in electrical engineering from the University of Oviedo, Gijón, Spain, in 2014.

He was a Research Fellow with the Department of Electrical Engineering, University of Oviedo, from October 2013 to June 2015. In July 2015, he joined the Department of Beams-RadioFrequency-Power Amplifiers and Modules Production (BE/RF/PM), European Organization for Nuclear Research (CERN), Geneva, Switzerland. He works on the construction and commission of electronic test benches for future medical applications. His research interests include reactive power compensation systems and power quality.

**Pablo Ardura G.** was born in Luarca, Spain, in 1986. He received the M.Sc. degree in electrical and electronic engineering from the University of Oviedo, Gijón, Spain, in 2010, where he is currently working toward the Ph.D. degree in electrical engineering.

From 2010 to 2014, he was with the Department of Electrical Engineering, University of Oviedo. In 2015, he joined the ArcelorMittal Global R&D Center Asturias, Avilés, Spain, where he is currently a Research Engineer. His research interests include power quality, power converters, energy storage, and waste-heat recovery systems for the steelmaking industry.

**José M. Cano** (M'98) was born in Oviedo, Spain, in 1971. He received the M.Sc. and Ph.D. degrees in electrical engineering from the University of Oviedo, Gijón, Spain, in 1996 and 2000, respectively.

In 1996, he joined the Department of Electrical Engineering, University of Oviedo, where he is currently an Associate Professor. During 2012, he was a Visiting Associate Professor at the Department of Electrical and Computing Engineering, The University of British Columbia, Vancouver, BC, Canada. His research interests include power quality solutions for industry, power converters, distributed generation, and smart grids.

**Joaquín G. Norniella** was born in Gijón, Spain, in 1980. He received the M.Sc. and Ph.D. degrees in electrical engineering from the University of Oviedo, Gijón, Spain, in 2005 and 2012, respectively.

He was a Research and Development Engineer with the Department of Electronic Engineering, University of Oviedo, for 20 months beginning in February 2007. In 2008, he joined the Department of Electrical Engineering, University of Oviedo, where he is currently a Lecturer. His research interests include power quality solutions for industry and power converters.

**Rocío Llera T.** was born in Oviedo, Spain, in 1983. She received the M.Sc. degree in forest and environment engineering from the University of Oviedo, Gijón, Spain, in 2006, where she is currently working toward the Ph.D. degree in mining, civil engineering, and project management.

She was a Research Engineer with the Department of Mining Exploitation, University of Oviedo, for four years beginning in 2006, working on environmental and energy topics in the steel sector. In 2010, she joined ArcelorMittal, Avilés, Spain, where she is currently an R&D Engineer with the Global R&D Center Asturias. Her research interests include energy issues focused on process modeling, waste energy recovery, and energy efficiency.

**Diego Cifrián R.** was born in Oviedo, Spain, in 1987. He received the M.Sc. degree in electrical engineering from the University of Oviedo, Gijón, Spain, in 2010.

In 2014, he joined ArcelorMittal, Avilés, Spain, where he is currently an R&D Engineer with the Global R&D Center Asturias. His research interests include innovative solutions for the steelmaking industry, focused on electrical and combustion process improvement.